

Coherence and Stimulated Emission in the Tavis-Cummings Model:
A Quantum Description of the Free Induction Signal and Radiation
Damping in Magnetic Resonance[†]

James Tropp

General Electric Healthcare Technologies

47697 Westinghouse Drive

Fremont CA, 94539

james.tropp@med.ge.com

[†] Preliminary accounts of this work were given at annual meeting of the International Society for Magnetic Resonance in Medicine (ISMRM), and at the Experimental NMR Conference (ENC), both in 2011.

Abstract

We numerically solve the Liouville equation for the Tavis-Cummings model of multiple spins coupled to a lossless single mode cavity, starting from an initial condition with small numbers of fully polarized spins ($N \leq 7$) tipped by a specified angle, and the cavity in its ground Fock state. Time evolution of the magnetizations and cavity states, following nutation of $\pi/2$ by a classical field, yields a microscopic quantum mechanical picture of radiation damping in magnetic resonance, and the formation of the free induction signal— that is, the transfer of Zeeman energy, via spin coherence, to cavity coherence. Although the motion of the Bloch vector is non-classical, our quantum description is related to the macroscopic picture of NMR reception, by showing the close relationship between the usual radiation damping constant, and the quantum mechanical Rabi nutation frequency (as enhanced by cavity coupling and stimulated emission.) That is, each is the product, of a nutation rate per oscillator current, and a current. Although the current in the damping constant is explicitly limited by cavity losses, which do not enter the formula for the Rabi frequency, we nonetheless show (in an appendix) how these losses can be introduced into our problem by means of a master equation. Numerical solution of the classical Bloch-Kirchhoff equations reinforces the conclusion that the strength of the free induction signal in magnetic resonance can only be accounted for by stimulated emission, in contrast to the generally accepted explanation based upon coherent spontaneous emission.

Introduction

Despite longstanding connections between quantum optics and nuclear magnetic resonance [1], NMR theoreticians –with the exception of those involved in force microscopy (or mechanical transduction more generally) [2, 3] -- have paid scant attention to the Jaynes-Cummings (J-C) model for the coupling of a two level atom (or a spin $\frac{1}{2}$) to a quantized cavity [4]; much less to that model's extension, by Tavis and Cummings (T-C), to accommodate multiple atoms or spins [5]. Recent work on the T-C model concerns the production and characterization of entangled states among Q-bits [6-8], and also the transition to semi-classical behavior [9-13]. But stimulated emission – while self evident from the form of the J-C Hamiltonian -- has not received comparable attention. Also, despite the importance of cavities driven by spins in coherent superpositions of stationary states [14-17], computational studies have often used simple inverted pure states (of high cooperation number) to drive the cavity [8-13, 17].

Here we apply the Tavis-Cummings model to magnetic resonance, specifically to NMR. Using the quantized LC circuit [18] as a stand-in for the cavity, we model the time course of Rabi oscillations for an NMR probe– initially in its ground state -- driven by several spins, coherently excited or simply inverted. NMR practitioners will find some of the results intuitive, and others less so. For example, despite showing the expected interchange of transverse and longitudinal magnetizations following a

nutations of $\pi/2$, the signal can exhibit quantum collapse and revival, i.e. damping and recovery through interference of isochromats of incommensurable frequencies [19, 20]. Also, driving the cavity with inverted spins gives Rabi oscillation of the longitudinal magnetization, with no transverse component developing, i.e. no detectable NMR signal. This reflects the fact that neither the T-C nor J-C Hamiltonian induces a pure rotation of the spins, which, in a loss free system, would conserve the length of the Bloch vector.

This non-rotational behavior of the quantum Bloch vector is pre-figured in the work of J-C [4], and also in the theory of micromasers [21-23], and does not conform to the semi-classical pendulum model [12, 24-26]. This fact gives rise to another counter-intuitive result, which will appear multiple times in the calculations to follow, namely that the longitudinal and transverse magnetizations evolve at different frequencies, offset by a factor of two, (with the transverse the slower.) In fact, what is conventionally called the ‘Rabi frequency’ is that for nutation of the longitudinal moment; and we will adhere to this usage.

As is well known, the optical Bloch equations, which *do* generate rotation of the spins, may be derived on the assumption of a cavity excited by a classical oscillatory field, or alternatively, a Glauber state [27-29]. But, while driving the cavity, initially quiescent, with a small number of spin coherences does produce coherences of the field, a fully formed Glauber state is not so quick to appear; nor have we seen it in any of our calculations.

Nonetheless, given that highly polarized ensembles of spins can produce multi-quantum coherences when excited with a single pulse [30, 31], higher coherences of the cavity field are readily demonstrated. (The

highly ordered and entangled spin states in these cases are usefully characterized using product-operator expansions [32-34] of the spin density matrix.)

In this paper, we will begin by presenting examples (as noted above) of the microscopic evolution of magnetizations and cavity fields, following suitable excitations. Then to help trace a path, from a microscopic theory of NMR transduction, to a realistic estimate of the macroscopic signal strength, we will calculate the cavity enhancement of Rabi oscillation, using the coupled oscillator model of J-C [4]. This, when combined with the twin motifs of spin coherence and stimulated emission, allows us to connect the Rabi nutation frequency with the usual (classical) radiation damping constant, and moves us towards a quantum description of the experimentally observed NMR signal, which has to date remained a work in progress [35-42].

Our model specifies a lossless cavity, since we believe that emission of a photon by a spin is the primordial event in signal formation, and that the eventual dissipative loss of that photon, following its initial capture by the cavity, is of lesser interest. Put another way, the phenomena associated with pure emission are sufficiently complex, that they deserve to be studied in isolation. Nonetheless, we do not ignore the important and difficult question of cavity losses; and a sketch of an appropriate master equation, and some calculational results, are given in an appendix.

Stimulated emission is essential to our argument, which runs counter to the conventional view that the rate of radiation damping is explained by coherent spontaneous emission, together with the high density of states inside a tuned cavity [43-46]. Of course, with a cavity starting in its ground state, the initiating event in reception (from a sample comprising multiple

spins) must always be spontaneous emission; but, as reception proceeds, and higher cavity states become populated, stimulated emission will assume primary importance in setting the observed signal power. In fact, from numerical solution of the classical Bloch-Kirchhoff equations, we estimate the contribution to signal power by stimulated emission at 60 dB, for protons in neat water at a Larmor frequency of 600 MHz.

The Case of Two Spins

The Tavis-Cummings Hamiltonian, in the interaction picture, is:

$$\mathfrak{H} = -\hbar \frac{\Omega_0}{2} \{ \hat{a}^\dagger (\hat{I}_+^{(1)} + \hat{I}_+^{(2)}) + \hat{a} (\hat{I}_-^{(1)} + \hat{I}_-^{(2)}) \} \quad [1]$$

where the Rabi frequency for the transition connecting the Fock states $|n\rangle$ and $|n+1\rangle$ is $\Omega_n = \sqrt{(n+1)}\Omega_0$, and Ω_0 is the Rabi fundamental; the operator pairings are for a spin $\frac{1}{2}$ with positive gyromagnetic ratio. The cavity operators for an LC circuit represent magnetic flux, but we will nonetheless call them field operators; this point is elaborated below. The basis set comprises product kets, e.g. $|n\alpha\beta\rangle$, giving the Fock state indices (0, 1, and 2) and the spin projections on the axis of quantization. The eigenvalues, in units of Ω_0 , are $\pm\sqrt{3/2}$, ± 1 , $\pm\sqrt{1/2}$, and 0 (multiplicity 6). The twelve members of the basis set include seven elements, which would together comprise a pair invariant subspaces of constant excitation 1

and 2 [47]; but a redundant basis is easily adaptable to the case of more spins and is therefore preferred.

Excited states of the spins are generated computationally by applying appropriate spin rotations ($\pi/2$ or π) to a preparatory density matrix $\rho^{(prep)} = |0\alpha\alpha\rangle\langle 0\alpha\alpha|$; it is considered that rotation is performed by a classical field, with which the spins do not become entangled; their subsequent time evolution, and entanglement with the cavity, is then determined by numerical solution of the Liouville equation. The form of $\rho^{(prep)}$ is appropriate for small numbers of spins, and also ensures a trace of unity. Since the cavity is presumed lossless, and the NMR linewidth perfectly homogeneous, excitation along the rotating axes x or y ensures that all off-diagonal elements of the reduced spin density matrix [19], $\rho^{(spin)}$, are either pure real or pure imaginary.

Since the descriptive matter to follow becomes dense, and since the conclusions are of necessity encumbered with supporting material, we take this opportunity to call attention to Figure 2A, which illustrates a central result: that is, a microscopic quantum description of radiation damping in NMR, and the formation of a detectable signal. Briefly, what is shown is the transfer (via spin coherence) of Zeeman energy from precessing spins to a tuned cavity, with the concomitant appearance of an induced field. We offer some caveats. The spins and cavity in our model are entangled, whereas in the semi-classical regime of ordinary NMR they are not. Also, since our model lacks dissipation, the cavity, once excited, re-excites the spins, and so on. These repetitive cycles of Rabi oscillation do not occur in the classical model of radiation damping [43], which assumes a highly damped cavity, in which evolution ends with the first zero crossing of the

transverse moment. Unfortunately, as we will later show, an entirely realistic theory, including cavity damping, is not readily achievable within the constraints of our present model, owing to the extreme smallness of typical damping times, relative to the Rabi nutation periods for the numbers of spins we deal with. Nonetheless, (as already noted) of the two competing processes in signal formation – emission and dissipation— we assign higher importance to the former, and treat latter as secondary. In this regard, another point of usage should be observed, pertaining to the distinction between radiation damping --the inclusive process whereby Zeeman energy is transferred to the cavity-- and cavity damping –the simple dissipative decay of that transferred signal. Details are given below; see particularly the second Appendix.

Figure 1A shows the time evolution of the magnetizations for two periods of the Rabi fundamental, starting from an initial condition in which both spins are tipped by $\pi/2$ and the cavity is in its ground state. The subsequent time course is calculated by evolving the propagator in the eigenbasis, following numerical diagonalization of the Hamiltonian [48]; individual spin and photon populations and coherences are then obtained from the corresponding reduced density matrices. The magnetizations are plotted at baseband, i.e. omitting the harmonic time dependence at the Larmor frequency (which strictly speaking, attaches to the spin operators in the interaction picture). All possible spin coherences are excited, of orders zero, one, and two, although only the latter two are visualized; the dotted trace shows the total number of excitations, constant and equal to 1.

The transverse magnetization (green trace) is a single-quantum coherence, normally giving rise to the NMR signal. Since our model

contains no dissipation, this oscillates repetitively (at $\sqrt{1/2}\Omega_0$) between the negative and positive x axes of the rotating coordinate frame [49]; in a normal NMR probe, as noted earlier, dissipation would restrict its motion to a single passage from its initial value to zero. We explicitly omit transverse relaxation, which in NMR is typically faster than radiation damping, and which would further restrict the trajectory of the transverse moment.

The longitudinal magnetization (blue trace) undergoes Rabi oscillation (starting from the value zero) at twice the frequency of the transverse (i.e. at the Rabi frequency.) Since the two magnetizations evolve at different frequencies, they cannot be said to be in time quadrature; nonetheless, the extrema of one occur at or near the zeros of the other, approximating the behavior expected for the time evolution of a free induction decay. The incipient damping, of both magnetizations, signals the onset of quantum collapse [20]; revival is easily demonstrated in a time course of longer duration.

The red trace (shown at doubled amplitude for better visualization) is the two-quantum coherence (a Schrödinger's cat state), which is given in product operator form as $\hat{I}_x^{(1)}\hat{I}_x^{(2)} + \hat{I}_x^{(1)}\hat{I}_x^{(2)}\hat{I}_z^{(1)}\hat{I}_z^{(2)}$, that is, the sum of zero and two quantum coherences, plus their difference. It oscillates (roughly sinusoidally) at the highest eigenfrequency, $\sqrt{3/2}\Omega_0$. (The two double products of z and x components commute.)

Figure 1B shows the time evolution of the cavity coherences (also at baseband.) There are two single quantum coherences (blue and green traces) with somewhat complicated time dependences, representing respectively the summed cavity reduced density matrix

elements $\rho_{12}^{(cavity)} \pm \rho_{21}^{(cavity)}$ (the sign positive for ρ real and negative for ρ

imaginary) and $\rho_{23}^{(cavity)} \pm \rho_{32}^{(cavity)}$, where the index 1 denotes the ground Fock state. The red trace, which undergoes approximately sinusoidal oscillation at $\sqrt{3/2}\Omega_0$, represents the two quantum coherence $\rho_{13}^{(cavity)} \pm \rho_{31}^{(cavity)}$; Fourier analysis shows that its time evolution tracks that of the corresponding spin coherence. The phase of the one quantum coherences depends upon the choice of axis for the initial excitation of the spins; for rotation about y (leading to purely real *spin* coherences, i.e. entirely expressed in terms of operator products, $I_x^{(i)}$ and $I_z^{(j)}$), the one quantum *cavity* coherences are pure imaginary. Real and imaginary components exchange when the excitation axis is rotated by $\pi/2$ about z . This is required to produce the $\sin \omega_0 t$ dependence of the induced fields, required classically by Faraday's law (ω_0 is the Larmor frequency), given the $\cos \omega_0 t$ dependence of the transverse magnetization in laboratory coordinates. Since the off-diagonal terms of the cavity reduced matrix are here purely imaginary, its trace with the summed field operators vanishes when the operator time dependence (at Larmor) is omitted. The summed operators may nonetheless be evaluated at Larmor, yet plotted at baseband, i.e. the phasor amplitude plotted, as is done below presently. Voltage and current are in phase for a perfectly tuned oscillator excited at resonance, and the net amplitude of flux – or field-- scales directly with current.

Summation of the pair of one-quantum cavity coherences (i.e. of the blue and green traces of Fig. 1B) removes the eccentric aspects of their time evolution, to yield the smooth (quasi-sinusoidal) waveform shown in dashed blue in Figure 2A. The transverse magnetization (cf Fig. 1A) is repeated (in green) for reference. The inset shows the Fourier analyses of the two

traces in magnitude format. The deviations from pure sinusoidal behavior result from the admixture of sums and differences of various eigenfrequencies: i.e. the major peaks are at $\sqrt{1/2}\Omega_0$; the minor peaks appear at the sum and difference frequencies with $\sqrt{3/2}\Omega_0$. Despite minor differences in frequency content, the two waveforms are approximately in time quadrature at baseband, as is expected for the transverse magnetization and the induced voltage, [50] in a conventional pulsed NMR experiment.

The dashed black trace gives the expectation value at baseband of magnetic flux (normalized to the square root of the occupation number), i.e. the summed field operators, $1/2(\hat{a}^\dagger + \hat{a})$, gotten as described above, by tracing with the reduced photon density matrix $\rho^{(cavity)}$. The time course of flux directly tracks that of the induced magnetic field. Since the transverse moment oscillates at about one half the Rabi frequency, and since our cavity is assumed lossless, the zero of transverse moment coincides with the maximum field, in contradistinction to the classical model, as noted below. The figure illustrates a model of NMR transduction, which we describe qualitatively as the conversion of spin coherence into cavity coherence.

For reference, Figure 2B shows the phenomena of collapse and revival –here of longitudinal magnetization -- observed over several periods of the Rabi fundamental, following preparation with a nutation pulse of $\pi/2$; following a π pulse no collapse occurs for two spins. The evolution in this latter case is a pure Rabi oscillation of the longitudinal magnetization, with no production of transverse magnetization or cavity coherence, which reconfirms the long-ago predictions of J-C [4]. Rabi oscillation occurs at a

frequency $2\Omega_0/\sqrt{2}$; the second strong peak responsible for the amplitude modulated character of the collapsing waveform is at $\sqrt{3/2}\Omega_0$.

Finally, we note that the free induction signal, for a single coherently excited spin driving a cavity in its ground state, may be gotten from the J-C model by an elementary analytic calculation. For completeness, these results are given (in density matrix formalism) in an appendix; they are qualitatively similar to those in Figures 1 and 2, except for the absence of collapse and revival. See also Figure 4 below. A pure-state description, of Rabi oscillation of a single coherently excited atom entering a cavity in its ground state, has also been sketched elsewhere, but without reference to the time course of the transverse moment, or to its quadrature phase relationship with the induced cavity field [15].

The Case of Multiple Spins ($N > 2$)

We restrict consideration to initial states similar to those above i.e. with $\rho^{(prep)} = |0\alpha\dots\alpha\rangle\langle 0\alpha\dots\alpha|$; the number of spins may reach 7. Figure 3A shows the time evolution of transverse magnetization, over a single period of the Rabi fundamental, for spin clusters with N ranging from two to seven, and the scale normalized correspondingly. The curves show the expected behavior, inasmuch as the decay rate of transverse magnetization (which essentially equals the emission rate in the semi-classical regime) grows with the number of emitted photons, and therefore demonstrates stimulated emission. The longitudinal magnetization (not shown) displays similar behavior, although not as pronounced.

Typical cavity dynamics are shown in Figure 3B, which gives, over the same time interval, (in solid lines) the time courses of the individual one-quantum cavity coherences, for five spins, – each calculated as above by summing conjugate elements), plus (in dashed blue) their net resultant, which exhibits the expected quasi-sinusoidal shape (cf Figure 2A), also with evidence of quantum collapse. The net magnetic flux (dashed black, calculated as describe earlier) tracks the total summed coherences. The rapid initial growth of cavity one-quantum coherence is explained by the early dominance of the 1,2 element (plus conjugate) in the cavity density matrix, which involves the cavity ground state – fully populated at the outset. The other tributaries (which we write in abbreviated form) -- e.g. $\rho_{23}^{(cavity)}$, $\rho_{34}^{(cavity)}$, $\rho_{45}^{(cavity)}$ – show the expected delayed growth characteristic of stimulated emission, as higher cavity levels are progressively populated.

The temporal dynamics of the free induction decay, and its decay by radiation damping, are further illustrated in Fig. 4A, which shows, for five spins in a single period of the Rabi fundamental, the interchange of the net photon population (red trace) with transverse (green) and longitudinal (blue) magnetizations. Again, in a typical NMR experiment, due to cavity losses, the process would end with the first zero crossing of transverse magnetization; but inasmuch as reception requires excitation of the cavity by the spins, the first half cycle of Rabi oscillation is the most important to us.

For comparison, we show in Figure 4B the analytic results for a single spin (cf Appendix A), for two periods of the Rabi fundamental. Apart from their higher symmetry, and slower evolution, these strongly resemble the numerical results, including the imaginary character of the cavity

coherences, which are in time quadrature with the spin coherence at the Larmor frequency, as is shown in Appendix I.

Cavity Enhancement and Stimulated Emission in NMR: the Rabi Frequency and the Radiation Damping Constant

We give first a numerical estimate of the cavity-enhanced Rabi fundamental, which fixes the temporal scale for all previous calculations. We then show that further enhancement of Rabi oscillation by stimulated emission leads (under the assumptions of our model) to the same nutation rate as that given the by the classical radiation damping constant. This links our microscopic quantum considerations to the observation of real NMR signals.

We follow the basic procedure of J-C [4], beginning with the details of the NMR antenna, considered as a quantized LC oscillator, where inductance and capacitance replace mass and spring constant. We modify the field operators defined by Louisell [18] (with canonical variables electric charge and magnetic flux) by multiplying with $\pm i$ (4, 51), to write the flux (i.e. canonical momentum) in terms of the inductance

as $\varphi = \sqrt{\hbar\omega_0 L/2}[\hat{a} + \hat{a}^\dagger]$. Postulating that the inductor comprises a singly wound Helmholtz pair, we approximate the laboratory frame B_1 field as $\varphi/2a$, where a is the window aperture in meters squared. This leads directly to the Rabi fundamental, i.e. $\Omega_0 = \gamma\sqrt{\hbar\omega_0 L/2}/2a$ and – taking higher matrix elements of the J-C Hamiltonian in Eq. [1] – to a Rabi frequency $\Omega_n = \gamma\sqrt{(n+1)\hbar\omega_0 L/2}/2a$ connecting the n th and $n+1^{\text{st}}$ Fock

states. (The constant $\sqrt{\hbar\omega_0 L/2}$ is effectively the flux per square root of the occupation number; the factor of $1/2$ required for the correct nutation rate is implicit in the partition of field operators according to the rotating wave approximation.)

Choosing a reasonable model for the Helmholtz pair, i.e. round windows of inside diameter 0.75 cm, separated by the diameter, we calculate an inductance of 58 nH, and a Rabi fundamental of $\Omega_0 = 8.13 \times 10^{-5} \text{ sec}^{-1}$ for a proton in a polarizing field of 14.1 tesla, i.e. with Larmor frequency ω_0 of 600 MHz. By contrast, the inverse lifetime for spontaneous emission at 600 MHz, by a single excited proton in free space, is:

$\mu_0 \hbar \gamma^2 \omega^3 / \pi c^3 = 6 \times 10^{-21} \text{ sec}^{-1}$. The staggering difference (~ 16 orders of magnitude) is due to the high concentration of magnetic flux created per photon, inside the coil, relative to that in free space. Jaynes and Cummings [4] calculated a smaller (yet still substantial) cavity enhancement of seven orders of magnitude for ammonia inversion in a beam-maser.

We now show that the classical radiation damping constant and the quantum-mechanical Rabi frequency are closely related. That is, each is the product of a nutation rate per cavity current, and a current, even though the damping constant includes cavity losses (which limit the final current) whereas with the Rabi frequency, in whose formulation losses do not enter, this limit is imposed simply by the number of spins. It suffices for our purposes to write the damping equation for the tip angle in the limit of small nutations, as $d\vartheta/dt = -k\vartheta$, where the damping constant is given without the troublesome filling factor, in terms of reciprocity theory [52-54]

as $k = \gamma \omega_0 V M_0 \zeta^2 / 4$, with the transceiver efficiency defined

as $\zeta = B_1(1)/\sqrt{R}$. Here $B_1(1)$ is the laboratory frame oscillatory B_1 field per ampere, and R is the coil resistance, without coupling to transceiver line impedance; M_0 is the equilibrium magnetization and V the sample volume. Thus the damping constant is a product of two factors: $\gamma B_1(1)/2$ and $\omega_0 V M_0 B_1(1)/2R$. The first is the nutation rate (in the rotating frame) per ampere of oscillator current; the second (by reciprocity) is just net the oscillator current (voltage over resistance). The coil resistance is effectively doubled here by critical coupling to the transceiver line. (The customary definition [43] of the damping constant in terms of the filling factor η , — $k = 2\pi\mu_0\gamma M_0 Q$, with $Q = \omega_0 L/R$ — may also be written as the product of a nutation rate per ampere and a current.)

We translate these results into quantum language by first noting that (under our earlier assumptions) the *rotating* frame B_1 field per unit oscillator current for our model NMR coil is just $L/4a$. We take the current (in a presumed semi-classical state) as given in terms of the mean occupation number [55] by $\sqrt{2n\hbar\omega_0/L}$, (according to $\frac{1}{2}LI^2 = n\hbar\omega_0$). The product of the field per current and the current, times the gyromagnetic ratio, is $\gamma\sqrt{n\hbar\omega_0 L/2}/2a$, which, for large n , is just the Rabi nutation frequency connecting the n th and $n+1^{\text{st}}$ Fock states, as obtained above. Viewed another way, transitions between higher states experience enhancement by stimulated emission, which may be calculated by scaling the Rabi fundamental by the square root of the occupation number, or, equivalently, the rate per unit current by the current.

The enhancement is substantial. As shown in the next section — for realistic damping currents, which may reach several milliamps for protons in

samples of neat water at 14.1 tesla– the occupation numbers are on the order of 10^{12} , leading to enhancements of six orders of magnitude over coherent spontaneous emission.

Finally, it is worth noting that we have, in the preceding, specified the usable field of the inductor, by applying a numerical factor to the flux – in this case a simple division by twice the coil aperture. A more complicated model, with a different numerical factor, could be chosen and carried throughout the argument, without affecting the generality of the result.

A Classical Model of Radiation Damping and the Free Induction Decay

The Bloch-Kirchhoff equations [43, 56-57] enable a realistic a calculation of the oscillator reception current, and therefore of the enhancement by stimulated emission. For a nuclear moment coupled to a lossy resonant coil, we find (ignoring relaxation) the following expression, for the magnetizations in the rotating frame, and for the in-phase and quadrature oscillator currents I_x and I_y :

$$\begin{bmatrix} \dot{I}_x \\ \dot{I}_y \\ \dot{M}_x \\ \dot{M}_y \\ \dot{M}_z \end{bmatrix} = \begin{bmatrix} -R/L & 0 & 0 & -\omega_0 V B_1(1)/2L & 0 \\ 0 & -R/L & \omega_0 V B_1(1)/2L & 0 & 0 \\ 0 & 0 & 0 & \Delta\omega & -\omega_{1y}(I_y) \\ 0 & 0 & -\Delta\omega & 0 & \omega_{1x}(I_x) \\ 0 & 0 & \omega_{1y}(I_y) & -\omega_{1x}(I_x) & 0 \end{bmatrix} \begin{bmatrix} I_x \\ I_y \\ M_x \\ M_y \\ M_z \end{bmatrix}$$

[2]

Here the matrix form of the Bloch equations follows Jaynes [58] (although for a nucleus of positive gyromagnetic ratio), and the oscillator portion is

derived from $LI + 2RI + \frac{1}{C} \int I dt = i\omega\mu_0 \mathbf{M} \cdot \mathbf{H}(1)$, by factoring out the time dependence of the current at the Larmor frequency, and discarding slowly varying terms [59]. The driving emf is written according to reciprocity [52, 53], assuming Maxwell's equations in time-harmonic form, with a negative sign chosen for the exponential time dependence. Dividing the H field by the harmonic current (to get the field per ampere) also removes its time dependence, so that H is treated as a constant when forming the various time derivatives. The resistance R is doubled (as above) by critical coupling to the transceiver line. The relative signs of the driving fields follow from relations between magnetizations and currents, given by Bloom [50]; these also may be gotten from reciprocity.

Figure 5 demonstrates realistic behavior for the radiation-damped free induction decay, following an initial tip of $\pi/2$. A similar calculation (not shown) with small tip angle (see above) gives a linewidth of 55 Hz after Fourier transformation. This compares reasonably with an experimental value of 65 Hz, measured for neat water on a probe whose sample volume, efficiency, and Q factor match those of the computational model [54]; refer to the figure legend for details. The ringing of the transverse moment is due to a resonance offset (introduced to show both quadrature components) and not to Rabi oscillation, of which the time course represents essentially a single half cycle.

From the familiar equation for Zeeman energy balance in terms of nutation angle ($\dot{E} = M_0 V B_0 \dot{\vartheta} \sin \vartheta$) we calculate, for $\dot{\vartheta} = \Omega_0$, a net power due to coherent spontaneous emission of 11 pW , that is, for nutation of the net moment at the Rabi fundamental, without stimulated emission.

This is far below the power of $25 \mu W$, calculated from Bloch-Kirchhoff with a peak oscillator current of 7 milliamps (cf Figure 5), and the given resistance. However, the oscillator occupation number for 7 milliamps is 3.57×10^{12} , yielding an increase in the Rabi frequency of a factor $\sqrt{n} = 1.9 \times 10^6$. The resultant power is $21 \mu W$, which lies within 20% of the power calculated classically. (In reckoning the classical power, the amplitude of the current must be treated as AC, and its rms value used. This is verified by a direct calculation in terms of the Zeeman energy, as gotten from the longitudinal moment.)

The numerical agreement between the two values of power ($21 \mu W$ and $25 \mu W$) is probably fortuitous, given the approximate nature of the calculations-- but it is nonetheless consistent with the view that the power in radiation damping has a substantial contribution, amounting to several orders of magnitude, from stimulated emission. This result is also consistent with the increase of the Rabi frequency measured in experiments on large populations of excited Rydberg atoms in a tuned cavity [60], as well for single atoms in the presence of larger injected fields [61].

The classical time course with dissipation amounts effectively to one half cycle of Rabi oscillation, in contrast to the earlier quantum results showing repetitive cycles. Presumably a realistic quantum model with damping of the cavity will (eventually) reproduce the classical result.

Discussion

In their classic work on radiation damping, Bloembergen and Pound [36] argued that the signal power observed in NMR— astronomically large compared to that of spontaneous emission – arises from two enhancement factors: the coherence of the ensemble of spins, and the increased radiation density inside a tuned cavity, as manifest in the cavity volume and its quality factor. This viewpoint has been accepted for decades [40].

Our calculations now suggest that these factors do not explain the strength of the FID signal —i.e. the rate of radiation damping— but that stimulated emission makes an essential contribution, amounting to several orders of magnitude. The treatment of the enhanced radiation density inside the cavity then becomes important, as we have followed here not Bloembergen-Pound, but Jaynes-Cummings [4].

That is, B-P, -- and others [43-46] -- typically write the field enhancement factor (the density of states) in terms of the cavity Q , as a measure the sharpness of the cavity resonance. This approach blurs the distinction between the atom-field coupling constant and the cavity dissipation rate, as set out in the bad cavity limit [62], and also as manifest in the master equation, which clearly separates the coherent atom-field interaction from the incoherent cavity damping.

J-C, in contrast, write the Hamiltonian directly in terms of the atom-field coupling constant, without reference to cavity dissipation. This also comports with the theory of reciprocity [52-54], inasmuch as the emf in nuclear magnetic resonance depends only upon the radiofrequency B field per unit oscillator current, which determines the nutation rate (i.e. Rabi frequency) given the actual current, and serves in the classical theory as an

analog to the coupling constant between spins and cavity. The J-C treatment is also intrinsically a theory of large nutations, in contrast to that of B-P, which relies on small perturbations, with the density of states entering through the Fermi Golden Rule.

Finally, we return to the question of rotations, raised briefly in the introduction above. The quantum Liouville equation for a spin $\frac{1}{2}$ coupled to a cavity can be written for the initial cavity state a Glauber state, in which case the Liouville matrix elements are diagonal in photon variables, and pure rotations of the Bloch vector can occur. Such conditions do not apply to our model, which starts with the cavity in its ground Fock state. But, inasmuch as a Glauber state is a solution for the undamped, driven quantum oscillator, we could perhaps anticipate, with enough spins and sufficient time, the development of a Glauber state, leading to a condition described classically by the Bloch or Bloch-Kirchhoff equations. Further calculations are needed, to verify this possibility, or not.

The disappearance of quantum collapse and revival has been proposed as a marker of the transition from quantum to classical behavior, in cavity quantum electrodynamics [10]. In the case of practical NMR where low resonator quality factors (~ 50 to 500) enforce the bad cavity limit, collapse and revival will simply not be observed; we therefore propose that the transition to classical behavior in NMR comes with the onset of rotation of the Bloch vector, i.e. which we take to coincide with the appearance of a cavity Glauber state. The current theory although incomplete, demonstrates the gap between the purely quantum and semi-classical regimes, with the latter corresponding to the customary world of NMR observations. Bridging the gap between the two will probably require calculations including both dissipation and many more spins.

However, we re-emphasize that with small numbers of spins, cavity coherence is limited strictly by the amount of spin coherence in the initial condition, and a pure inversion of the spins results in Rabi oscillation of longitudinal magnetization, i.e. direct transfer of Zeeman energy into Fock states without the intervention of spin coherence. This is not predicted by the Bloch-Kirchoff model, nor is adding it as an ad hoc correction fully satisfactory [12]. Given that the rate of decay should be comparable to that of normal radiation damping — on the order of 50 sec^{-1} for neat water at 600 MHz — and therefore much faster than longitudinal relaxation, this effect should be measureable in a conventional NMR experiment, in the interval following spin inversion, and before the advent of the noise triggered free induction decay [63]. Since transfer of energy should occur without development of an induction signal, this phenomenon might reasonably be called ‘radiationless damping.’

Acknowledgement

This work was supported by General Electric Healthcare Technologies.

Appendix I: Analytical Results for the Jaynes-Cummings Model

We outline here the solution of the J-C problem for a single spin, nutated by $\pi/2$, interacting with a cavity in its ground Fock state. The basis elements are the simple products $|0\alpha\rangle, |0\beta\rangle, |1\alpha\rangle$. The starting density matrix (with the spin tipped) is:

$$\rho^{(init)} = 1/2 \begin{bmatrix} 1 & 1 & 0 \\ 1 & 1 & 0 \\ 0 & 0 & 0 \end{bmatrix} . \quad \text{A1}$$

Then with the abbreviations $c = \cos \frac{1}{2} \Omega_0 t$ and $s = \sin \frac{1}{2} \Omega_0 t$, the density matrix at time t is:

$$\rho(t) = 1/2 \begin{bmatrix} 1 & c & -is \\ c & c^2 & -isc \\ is & isc & s^2 \end{bmatrix} . \quad \text{A2}$$

The reduced spin and photon density matrices are:

$$\rho^{(spin)}(t) = 1/2 \begin{bmatrix} 1+s^2 & c \\ c & c^2 \end{bmatrix} . \quad \text{A3}$$

and

$$\rho^{(cavity)}(t) = 1/2 \begin{bmatrix} 1+c^2 & -is \\ is & s^2 \end{bmatrix} . \quad \text{A4}$$

From these expressions it is easily seen that the longitudinal magnetization oscillates at the Rabi frequency, and the transverse at one half that value; also (as detailed below) that the cavity one quantum coherence and transverse magnetization are in time quadrature in the laboratory frame. This behavior mirrors that observed for multiple spins, except that collapses and revivals are not seen in this simple case. The case of an initial nutation

of π is easily worked out, and shows a perfect absence of transverse magnetization. Comparison of the off diagonal elements of the reduced density matrices reveals a dual hierarchy of in phase and quadrature components. The appearance of imaginary values in one but not the other reflects a quadrature phase shift at the carrier frequency; the fact that one is expressed as a sine and the other as a cosine shows an additional quadrature relationship existing at baseband.

Appendix II: An Approach to a Treatment of Cavity Losses

We here present, not a definitive solution to the problem of cavity losses in radiation damping, but rather, a sketch of the path by which we think the solution will eventually be found, together with some indicative computational results. The subject is not new, but little has been written.

Earlier quantum mechanical treatments of spins in cavities have incorporated cavity damping by a transmission line dashpot [38, 64], without introducing explicit cavity losses. Another approach [39] starts with the Bloch-Kirchoff equations, written in terms of the magnetizations, but arrives at a damping equation derived from the theory of superfluorescence [24, 25], in which photons are lost not by dissipation, but by escape from an active volume; the final equations are written purely in terms of spin operators, without the presence of cavity operators. Apart from the inconvenient products of magnetizations at the outset, this appears satisfactory in the semi-classical regime, when the spins and the cavity are not entangled. However, under the conditions of a pure quantum description, including entanglement, we think it best to apply a very different method, which we borrow from the theory of micromasers.

The starting point is clearly some form of master equation, embodying both coherent and stochastic evolution. In this context, it is worth pointing out what is rarely remarked, that is the similarity between the usual master equation in quantum optics [65], and the Bloch-Wangsness-Redfield equation [66, 67] in magnetic resonance. In fact the standard derivation of cavity losses will be easily followed by anyone familiar with Redfield theory [67]. This derivation has been given elsewhere in too much detail to be here repeated [21-23, 65], but we summarize a few salient points.

The goal is to introduce cavity losses quantum mechanically, which is done by means of a coupling Hamiltonian, which links the cavity to a thermal bath of quantum oscillators. This Hamiltonian contains only field operators, and therefore commutes with the Zeeman Hamiltonian. The corresponding Liouville equation is then solved to second order in perturbation, and suitable ensemble averages are performed over fluctuating quantities. The resultant for $\dot{\rho}$ contains an iterated commutator, which, when, expanded, takes the form:

$$\dot{\rho} = (\gamma/2)\{(n+1)(2\hat{a}\rho\hat{a}^\dagger - \hat{a}^\dagger\hat{a}\rho - \rho\hat{a}^\dagger\hat{a}) + n(2\hat{a}^\dagger\rho\hat{a} - \hat{a}\hat{a}^\dagger\rho - \rho\hat{a}\hat{a}^\dagger)\},$$

(A5)

where n is the mean photon occupation number, and γ the photon damping rate. In quantum optics, ρ is often the reduced photon density matrix [21], but here it is the combined spin-photon matrix, with the cavity operators written as Kronecker products with the spin identity operator. This damping term is then added to the normal Liouville equation containing the T-C Hamiltonian, to give the full master equation with damping.

This we have solved numerically for the simple initial condition of two spins inverted (i.e. with zero coherence), to give the result shown in Figure 6. Given that the time scale is normalized to the Rabi fundamental, the photon damping rate was chosen (empirically) as 0.8. Then the cavity damping is mostly clearly seen in the slow decrease of the total excitations (dotted trace), which, absent dissipation, would remain at a constant value of two. The irregular downward progress tracks the mean photon occupation number, in accord with Eq. A5. Comparison to Fig. 2B also shows that the longitudinal magnetization (blue trace, Fig. 6)-- which, following an initial nutation of π , oscillates without decay in a lossless cavity-- now undergoes a quite notable decrement, over the two periods shown of the Rabi fundamental. Likewise the total photons (red trace.) The transverse magnetization (green) is included in the figure to re-emphasize a point made before, and well known in the theory of micromasers, that an inverted spin, undergoing Rabi nutation according to the Jaynes-Cummings Hamiltonian, does not acquire a transverse moment.

These results are suggestive, but the photon decay rate is far, far slower than that observed in ordinary NMR probes at ambient temperatures. This is shown by reference to Fig. 5, where a realistic model places the Rabi period on the order of seconds, while the cavity decay time lies in the microsecond range. The effective damping rate scales as the mean photon occupation number, which, in the present calculation, never exceeds 2; whereas in a model with the cavity at room temperature, it could be expected to be of the order of $kT/h\nu$ at the outset of reception -- typically around 10^5 --and then to further grow as reception proceeded. Such a rate would completely preclude the observation of Rabi nutation in

our model; and so an approach to a more realistic simulation might involve many more spins, and a thermal bath of a few degrees Kelvin. We believe that what we have shown is nonetheless of interest, in suggesting a reasonable path, and the likely difficulties to be encountered.

Figure Legends

Figure 1: Two spins in a single-mode cavity: time evolution of magnetizations and photon coherences, over two periods of the Rabi fundamental, following a $\pi/2$ pulse of the spins from an initial state of perfect polarization. The amplitudes are viewed at base band, so their time dependence reflects only the T-C coupling. Spin and photon coherences are offset in time by one quarter period, i.e. a phase shift of $\pi/2$, negligible compared to the Rabi period. A) Longitudinal magnetization (blue), transverse magnetization (green), two quantum coherence (red.). Vertical axis normalized to number of spins. The dotted black line is the number of excitations, constant at 1.0. B) Individual one-quantum cavity coherences: $\rho_{12}^{(cavity)} \pm \rho_{21}^{(cavity)}$ (blue) and $\rho_{23}^{(cavity)} \pm \rho_{32}^{(cavity)}$ (green); and also two quantum cavity coherence $\rho_{13}^{(cavity)} \pm \rho_{31}^{(cavity)}$ (red). Due the phase offset at the Larmor frequency, these are pure imaginary, so of each conjugate pair of density matrix elements, only one is member is plotted.

Figure 2. A) For two spins, prepared as in Figure 1, time course over two Rabi periods, of transverse magnetization (green, vertical axis normalized to number of spins.), and (in dotted blue, un-normalized) summed one quantum cavity coherences (blue and green from Figure 1B.) Also, dotted black, the normalized magnetic flux (per square root photon), obtained by tracing the reduced photon density matrix with the field operator. The sum represents the net one quantum coherence, and measures the electromagnetic field in the cavity. The insets give the corresponding Fourier analyses in

magnitude format. Further explanation in text. B) For two spins, time course of longitudinal magnetization following pulse of $\pi/2$ (above) and π (below), for 10 periods of the Rabi fundamental. Fourier analyses inset; further explanations in text. Quantum collapse and revival are clearly seen in the upper trace, although not the lower. *Note the division of the vertical scale for the upper and lower traces.*

Figure 3. A) Illustration of stimulated emission over one period of the Rabi fundamental: time courses of transverse magnetization for increasing numbers of spins, from two – (solid blue trace) through seven (dotted red trace.) (Number of spins increases in color sequence blue, green, red, and from solid to dotted trace) The damping (emission) rate is indicated by the first zero crossing, which arrives progressively sooner with each additional spin, as expected from stimulated emission. Vertical axis normalized to number of spins. B) One quantum cavity coherences (solid traces) for five spins, and their summations, to give approximately sinusoidal resultant (dashed navy trace); also, the dashed black trace gives net flux, gotten as described for Fig. 2. Color sequence of one quantum coherences (solid lines) starting from $\rho_{12}^{(cavity)} \pm \rho_{21}^{(cavity)}$ is navy, red, green, violet, cerulean. Note the acceleration relative to two spins shown in Figure 2. Refer to text for details.

Figure 4. A) Signal formation and radiation damping with five spins, following nutation of $\pi/2$, for one period of the Rabi fundamental. Transverse and longitudinal magnetizations (green and blue), total photons (red), and total excitations (dashed black.) B) Results of analytical solution

of Jaynes-Cummings problem for a single spin in cavity tuned to the Larmor frequency, following nutation of $\pi/2$, for *two* periods of the Rabi fundamental. Color code as in part A. Note the strong qualitative resemblance between A and B, and also the relative slowness of the process for one spin. Note also the damping in A due to quantum collapse, absent in B.

Figure 5. A) For the model coil described in the text, calculated FID for small initial small tip – in phase (diamonds) and quadrature (triangles) transverse moments in amp/meter², also longitudinal moment (dashed) -- in rotating frame, with resonance offset 150 Hz, which gives rise to the ringing of the transverse moments. Details of the sample and the measurement of the coil efficiency are chosen to match *experimental* conditions in reference [50]. The starting magnetic moment is $9.73 \times 10^{-9} \text{ amp} - \text{meter}^2$ amp-meter², corresponding to neat water in a 5 mm NMR tube with a vertical probe window of height 1.6 cm, at $T = 298 \text{ K}$. The RF coil efficiency was measured at $1.92 \times 10^{-4} \text{ tesla}/\sqrt{\text{watt}}$. This, combined with the *measured* quality factor of $Q = 220$ plus an *assumed* coil resistance of $R = 0.5 \text{ ohm}$, leads to a coil inductance $L = 58 \text{ nH}$, B) Time course peak oscillator current at baseband for FID in A above. Note the early time point near zero current, followed by the sharp drop to -7 mA ; this is the start up transient of the coil, which is also illustrated in the inset, and which has a total time duration of 1 microsecond, and a vertical excursion equal to that of the larger figure.

Figure 6. Evolution of two spins in a lossy cavity, following initial nutation of π . The vertical scale is normalized to the number of spins. Longitudinal and transverse magnetizations are shown in blue and green respectively, total photons in red, and total excitations in dashed black. The full spin-cavity density matrix is numerically evolved under the master equation, and the reduced spin and cavity matrices then evaluated, from which the displayed quantities are gotten. The decay of the total excitations occurs not at a constant rate, but fluctuates according to the mean photon occupation number (red trace.)

References

1. N. Bloembergen, "Nonlinear Optics", 4th Edn. World Scientific Publishing (Singapore) 1996.
2. J. A. Sidles, Phys. Rev. Lett. **68**, 1124 (1991).
3. I. Bargatin and M. L. Roukes, Phys. Rev. Lett. **91**, 138302 (2003); M. C. Butler, V. A. Norton, D. P. Weitekamp, Phys. Rev. Lett. **105**, 177601 (2010).
4. E. T. Jaynes and F. W. Cummings, Proc. IEEE **51**, 89 (1963).

5. M. Tavis and F. W. Cummings, Phys. Rev. **170**, 379 (1968).
6. A. Retzker, E. Solano, and B. Reznik, Phys. Rev. A **75**, 022312 (2007).
7. J. M. Fink, R. Bianchetti, M. Baur, M. Go., L. Steffen, S. Filipp, P. J. Leek, A. Blais, and A. Wallraff, Phys. Rev. Lett. **103**, 083601, (2009).
8. T. E. Tessier, I. H. Deutsch, and A. Delgado, Phys. Rev. A **68**, 062316 (2003).
9. J. M. Fink, L. Steffen, P. Studer, Lev S. Bishop, M. Baur, R. Bianchetti, D. Bozyigit, C. Lang, S. Filipp, P. J. Leek, and A. Wallraff, Phys. Rev. Lett. **105**, 163601, (2010).
10. M. J. Everitt, W. J. Monroe, and T. P. Spiller, Phys. Rev. A **79**, 032238 (2009).
11. J. Keeling, Phys. Rev. A **79**, 053825 (2009).
12. R. Bonifacio and G. Preparata, Phys. Rev. A, **2**, 336 (1970).
13. R. H. Dicke, Phys. Rev., **93**, 99 (1956).
14. J. J. Slosser, P. Meystre, and S. L. Braunstein, Phys. Rev. Lett. **9**, 934, (1989); J. J. Slosser, P. Meystre, and E. M. Wright, Opt. Lett. **15**, 223, (1989).

15. J. Raimond, H. Brune, and S. Haroche, *Rev. Mod. Phys.* **73**, 565 (2001).
16. R. H. Mabuchi and A.C. Doherty, *Science* **298**, 1372 (2002).
17. M. Kozirowski, S. M. Chumakov, J. Swiatlowski and A. A. Mamedov, *Phys. Rev. A* **46**, 7220 (1992).
18. W. H. Louisell, *Quantum Statistical Properties of Radiation*, Wiley, New York. 1990 Ch. 4.
19. F. W. Cummings, *Phys. Rev.* **140**, A1051 (1965); E. T Jaynes, *Phys. Rev.* **108**, 171 (1957).
20. J. H. Eberly, N. B. Narozhny, and J. J. Sanchez-Mondragon, *Phys. Rev. Lett.* **44**, 1323, (1980).
21. P. Filipowicz, J. Javanainen, and P. Meystre, *Phys. Rev. A* **34**, 3077, (1986).
22. A. Lugiato, M. O. Scully, and H. Walther, *Phys. Rev. A* **36**, 740, (1987).
23. B-G. Englert, arXiv:quant-ph/0203052v1 13 Mar 2002
24. R. Bonifacio and L. A. Lugiato, *Phys. Rev. A* **11**, 1507, (1975).
25. R. Bonifacio and L. A. Lugiato, *Phys. Rev. A* **12**, 587, (1975).

26. L. Moi, P. Goy, M. Gross, J. M. Raimond, C. Fabre, and S. Haroche, *Phys. Rev. A* **27**, 2043, (1983).
27. D. F. Wallis and G. J. Milburn, *Quantum Optics*, Springer, Berlin, 1994 p 215.
28. P. L. Knight and P. W. Milonni, *Physics Reports* **66**, 21 (1981).
29. H. Mabuchi, *Phys. Rev. A* **78**, 015801, (2008).
30. J. S. Waugh, O. Gonen, and P. Kuhns, *J. Chem Phys.* **86**, 3816 (1987).
31. Q. He, W. Richter, S. Vatyam, and W. S. Warren, *J. Chem. Phys.* **98**, 6779 (1993).
32. U. Fano, *Rev. Mod. Phys.* **29**, 74 (1957).
33. N. C. Pyper, *Mol. Phys.*, **21**, 1 (1971).
34. O. W. Sørensen, G. W. Eich, M. H. Levitt, G. Bodenhausen, and R. R. Ernst, *Prog. Nucl. Magn. Reson. Spectrosc.*, 1983, 16, 163.
35. J. Jeener and F. Henin, *Phys. Rev. A*, **34**, 4897 (1986).
36. M. A. McCoy and W. S. Warren, *J. Chem. Phys.* **93**, 858 (1990).

37. D. Abergel, M. L. Delsuc and J-Y. Lallemand, J. Chem. Phys. **96**, 1657 (1990).
38. J. Jeener and F. Henin, J. Chem Phys. **116**, 8036 (2002).
39. D. Abergel, and J-Y. Lallemand, J. Magn. Reson. Series A **110**, 45 (1994).
40. D. I. Hoult and N. S. Ginsburg, J. Magn. Reson. **148**, 182, (2001).
41. M. Giordano, D. Leporini, M. Martinelli, S. Santucci, and C. Umeton, Phys. Rev. A **38**, 1931 (1988).
42. G. J. Boender, S. Vega, and H. J. M. de Groot, J. Chem Phys. **112**, 1096, (2000).
43. N. Bloembergen and R. V. Pound, Phys. Rev. **95**, 8 (1954).
44. D. Kleppner, Phys. Rev. Lett. **47**, 233, (1981).
45. P. Goy, J. M. Raimond, M. Gross, and S. Haroche, Phys. Rev. Lett. **50**, 1903 (1983).
46. H. Walther , B. T. H. Varcoe , B.-G. Englert and T. Becker, Rep. Prog. Phys. **69** (2006) 1325.
47. zeng arXiv:quant-ph/0106020v1.

48. G. Ramon, C. Brif, and A. Mann, *Phys. Rev. A* **58**, 2506 (1998).
49. I. I. Rabi, N. Ramsey and J. Schwinger, *Rev. Mod. Phys.* **26**, 167 (1954),
50. S. Bloom, *J. Appl. Phys.* **28**, 800 (1957).
51. P. A. M. Dirac *Quantum Mechanics*, 3rd Edition, (Oxford, Clarendon Press, 1947) Ch. VI.
52. D.I. Hoult, R.E. Richards, *J. Magn. Reson.* **24** 71 (1976).
53. J. Tropp, *Phys. Rev. A* **74** 062103 (2006).
54. J. Tropp and M. Van Crielinge, *J. Magn. Reson.*, **206** 161, (2010).
55. K. Gottfried and T-M. Yan, *Quantum Mechanics: Fundamentals*, (Springer Verlag, Berlin. 2003) p 183.
56. P. Bösiger, E. Brun, and D. Meier, *Phys. Rev. A* **18**, 671, (1978); R. Holzner, B. Derighetti, M. Ravani, and E. Brun, *Phys. Rev. A* **36**, 1280, (1987).
57. B. Derighetti, M. Ravani, R. Stoop, P. F. Meier, and R. Badii, *Phys. Rev. Lett.* **55**, 1746, (1985); E. Brun, B. Derighetti, D. Meier, R. Holzner, and M. Ravani, *J. Opt. Soc. Am B.* **2**, 156, (1985).

58. E. T. Jaynes, Phys. Rev. **98**, 1099 (1955).
59. H. Haken, *Laser Theory*, (Springer Verlag, Berlin. 1983) p 178-79 .
60. Y. Kaluzny, P. Goy, M. Gross, J. M. Raimond, and S. Haroche, Phys. Rev. Lett. **51**, 1175 (1983).
61. M. Brune, A. Maali, J. Dreyer, E. Hagley, J. M. Raimond, and S. Haroche, Phys. Rev. Lett. **76**, 1800 (1996).
62. P. R. Rice and H. J. Carmichael, IEEE J. Quantum Electronics, **24**, 1351 (1988).
63. M. P. Augustine, S. D. Bush, and E. L. Hahn, Chem. Phys. Lett. **322**, 111, (2000).
64. K. W. H. Stevens, Proc. Physical Society **77**, 515 (1961).
65. Louisell, *op. cit.*, Ch. 6; C. W Gardiner and P. Zoller , *Quantum Noise*, 2nd Edition, (Springer Verlag, Berlin, 2000), Ch. 5.
66. R. K. Wangsness and F. Bloch, Phys. Rev. **89**, 728, (1953).
67. A. G. Redfield, in “Advances in Magnetic Resonance,” (J. S. Waugh, Ed.) Vol. 1, 1 Academic Press, New York, 1965.

Figures for Reference

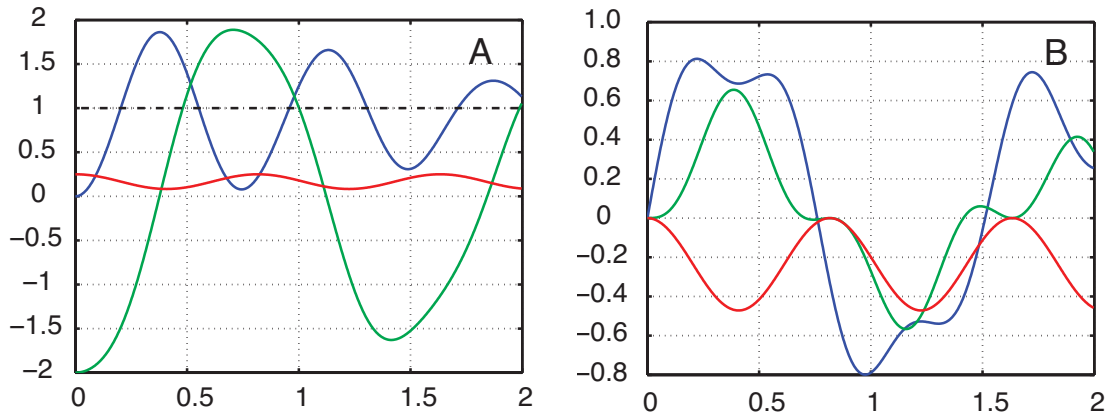


Figure 1: Two spins in a single-mode cavity: time evolution of magnetizations and photon coherences, over two periods of the Rabi fundamental, following a $\pi/2$ pulse of the spins from an initial state of perfect polarization. The amplitudes are viewed at base band, so their time dependence reflects only the T-C coupling. Spin and photon coherences are offset in time by one quarter period, i.e. a phase shift of $\pi/2$, negligible compared to the Rabi period. A) Longitudinal magnetization (blue), transverse magnetization (green), two quantum coherence (red.). Vertical axis normalized to number of spins. The dotted black line is the number of excitations, constant at 1.0. B) Individual one-quantum cavity coherences: 1,2 (blue) and 2,3 (green); and also two quantum cavity coherence 1,3 (red). Due the phase offset at the Larmor frequency, these are pure imaginary, so of each conjugate pair of density matrix elements, only one is plotted.

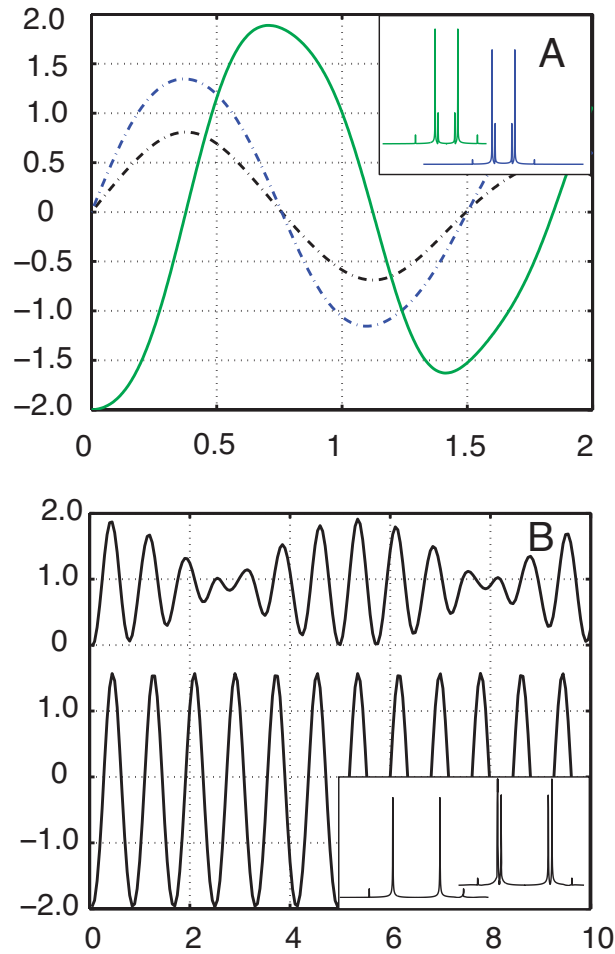


Figure 2. A) For two spins, prepared as in Figure 1, time course over two Rabi periods, of transverse magnetization (green, vertical axis normalized to number of spins.), and (in dotted blue, un-normalized) summed one quantum cavity coherences (blue and green from Figure 1B.) Also, dotted black, the normalized magnetic field (per square root photon), obtained by tracing the reduced photon density matrix with the field operator. The sum represents the net one quantum coherence, and measures the electromagnetic field in the cavity. The insets give the corresponding Fourier analyses in magnitude format. Further explanation in text. B) For two spins, time course of longitudinal magnetization following pulse of $\pi/2$ (above) and π (below), for 10 periods of the Rabi fundamental. Fourier analyses inset; further explanations in text. Quantum collapse and revival are clearly seen in the upper trace, although not the lower. *Note the division of the vertical scale for the upper and lower traces.*

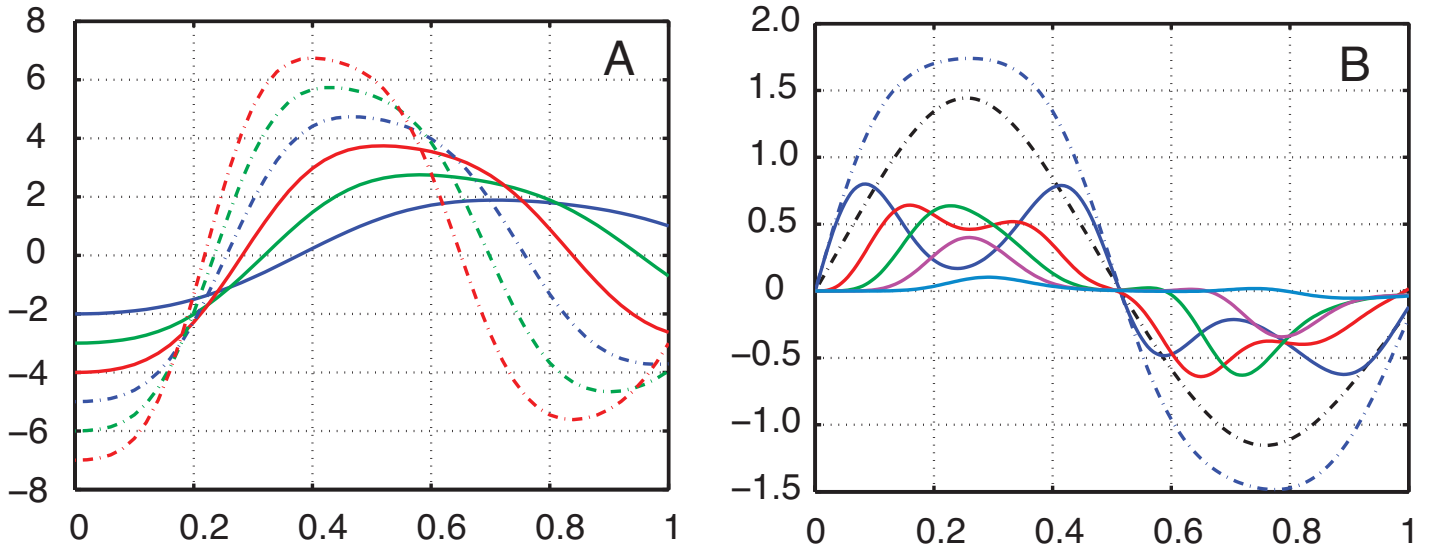


Figure 3. A) Illustration of stimulated emission over one period of the Rabi fundamental: time courses of transverse magnetization for increasing numbers of spins, from two – (solid blue trace) through seven (dotted red trace.) (Number of spins increases in color sequence blue, green, red, and from solid to dotted trace) The damping (emission) rate is indicated by the first zero crossing, which arrives progressively sooner with each additional spin, as expected from stimulated emission. Vertical axis normalized to number of spins. B) One quantum cavity coherences (solid traces) for five spins, and their summations, to give approximately sinusoidal resultant (dashed navy trace); also, weighted sum (dashed black trace) gives net flux. Color sequence of one quantum coherences (solid lines) starting from $\rho_{12}^{(cavity)}$ is navy, red, green, violet, cerulean. Note the acceleration relative to two spins shown in Figure 2. Refer to text for details.

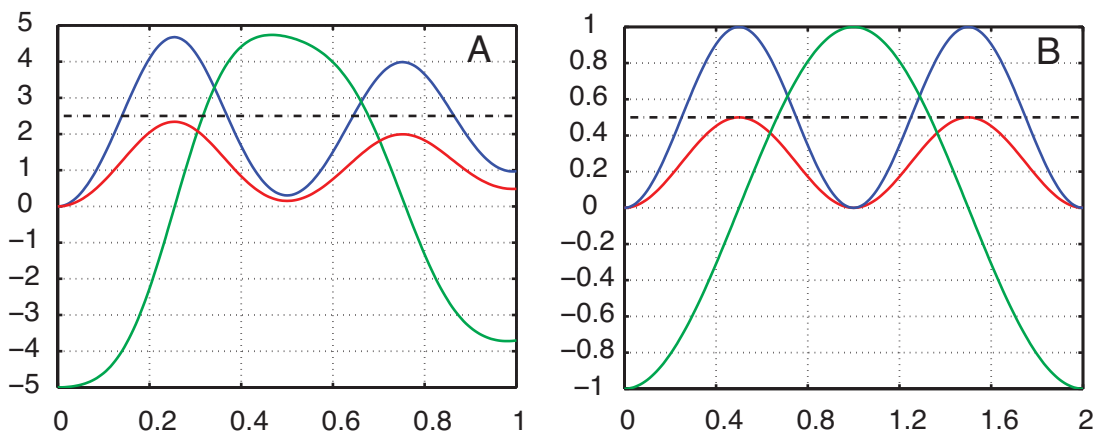


Figure 4. A) Signal formation and radiation damping with five spins, following nutation of $\pi/2$, for one period of the Rabi fundamental. Transverse and longitudinal magnetizations (green and blue), total photons (red), and total excitations (dashed black.) B) Results of analytical solution of Jaynes-Cummings problem for a single spin in cavity tuned to the Larmor frequency, following nutation of $\pi/2$, for *two* periods of the Rabi fundamental. Color code as in part A. Note the strong qualitative resemblance between A and B, and also the relative slowness of the process for one spin. Note also the damping in A due to quantum collapse, absent in B.

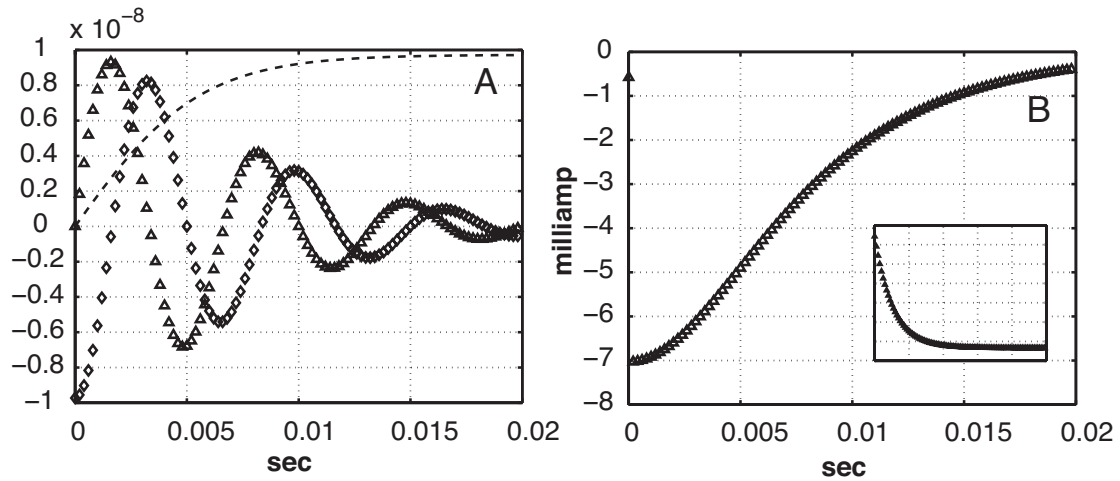


Figure 5. A) For the model coil described in the text, calculated FID for initial tip of $\pi/2$ – in-phase (diamonds) and quadrature (triangles) transverse moments in amp/meter², also longitudinal moment (dashed) -- in rotating frame, with resonance offset 150 Hz, which gives rise to the ringing of the transverse moments. Details of the sample and the measurement of the coil efficiency are chosen to match *experimental* conditions in reference [50]. The starting magnetic moment is $9.73 \times 10^{-9} \text{ amp} - \text{meter}^2$, corresponding to neat water in a 5 mm NMR tube with a vertical probe window of height 1.6 cm, at $T = 298 \text{ K}$. The RF coil efficiency was measured at $1.92 \times 10^{-4} \text{ tesla}/\sqrt{\text{watt}}$. This, combined with the *measured* quality factor of $Q = 220$ plus an *assumed* coil resistance of $R = 0.5 \text{ ohm}$, leads to a coil inductance $L = 58 \text{ nH}$, B) Time course peak oscillator current at baseband for FID in A above. Note the early time point near zero current, followed by the sharp drop to -7 mA; this is the start-up transient of the coil, which is also illustrated in the inset, which has a total time duration of 1 microsecond, and a vertical excursion equal to that of the larger figure.

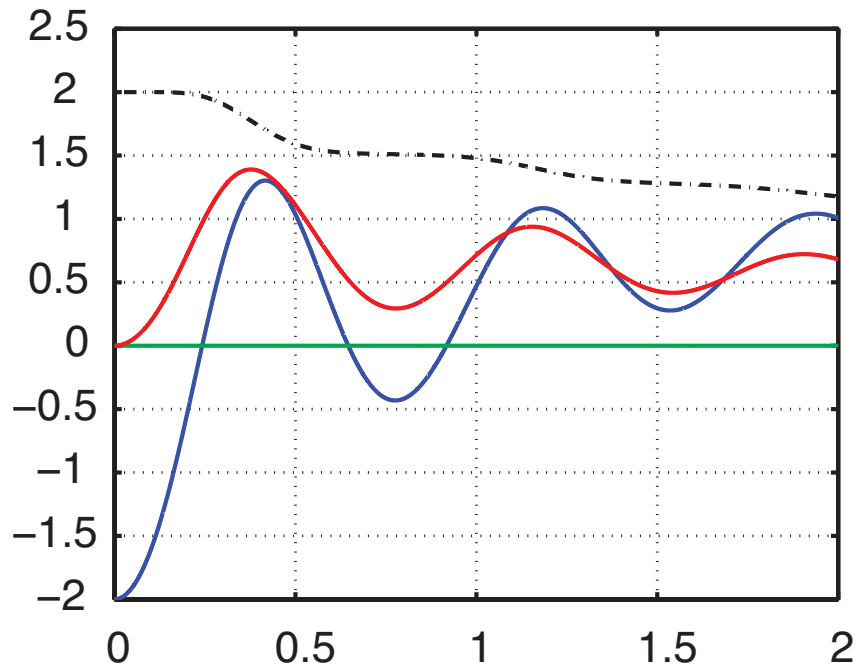


Figure 6. Evolution of two spins in a lossy cavity, following initial nutation of π . The vertical scale is normalized to the number of spins. Longitudinal and transverse magnetizations are shown in blue and green respectively, total photons in red, and total excitations in dashed black. The full spin-cavity density matrix is numerically evolved under the master equation, and the reduced spin and cavity matrices then evaluated, from which the displayed quantities are gotten. The decay of the total excitations occurs not at a constant rate, but fluctuates according to the mean photon occupation number (red trace.)